



Contents lists available at ScienceDirect

Mechanical Systems and Signal Processing

journal homepage: www.elsevier.com/locate/ymssp

Application of cyclic coherence function to bearing fault detection in a wind turbine generator under electromagnetic vibration



Wei Teng^{a,*}, Xian Ding^a, Yangyang Zhang^a, Yibing Liu^a, Zhiyong Ma^a,
Andrew Kusiak^b

^a School of Energy, Power and Mechanical Engineering, North China Electric Power University, Beijing 102206, China

^b Mechanical and Industrial Engineering, The University of Iowa, Iowa City, Seamans Center, 3131, IA 52242-1527, USA

ARTICLE INFO

Keywords:

Cyclic coherence function
Bearing fault
Wind turbine generator
Electromagnetic vibration

ABSTRACT

In a wind turbine generator, there is an intrinsic electromagnetic vibration originated from an alternating magnetic field acting on a low stiffness stator, which modulates vibration signals of the generator and impedes fault feature extraction of bearings. When defects arise in a bearing, the statistics of the vibration signal are periodic and this phenomenon is described as cyclostationarity. Correspondingly, cyclostationary analysis enables finding the degree of cyclostationarity representing potential fault modulation information. In this paper, the electromagnetic vibration acting as a disturbance source for fault feature extraction is deduced. Additionally, the spectral correlation density and cyclic coherence function used for vibration analysis are estimated. A real 2 MW wind turbine generator with a faulty bearing was tested and the vibration signals were analyzed separately using conventional demodulation analysis, cyclic coherence function, complex wavelet transform and spectral kurtosis. The analysis results have demonstrated that the cyclic coherence function can detect the fault feature of inner race successfully, while the feature is concealed by intensive electromagnetic vibration in the other three methods. The disassembled bearing of the wind turbine generator illustrates the effectiveness of the analysis result, and precautionary measures for protecting bearings in generators are suggested.

1. Introduction

Wind energy plays a significant role in renewable energies worldwide. Especially in China, 30.8 GW of new installed capacity was increased in 2015, once again the highest annual number for any country ever [1]. Meanwhile, the reliability and safety of wind turbines are attracting more and more attentions from both operators and manufacturers because of their decisive effect on operation cost and power efficiency [2]. As a result of suffering extreme temperature difference and alternating loads, a wind turbine drive train which consists of a rotor hub, a gearbox and a generator easily fails making its health conditions necessary to be monitored and diagnosed duly [3–5].

The generator is positioned on the end of the wind turbine drive train. High rotational speed, electromagnetic vibration, misalignment with the gearbox and shaft current corrosion etc. may damage stator winding, rotor winding or the bearing in the generator. In wind turbine generators greater than 1 MW, the bearing is the most frequent failure part [6], which can induce catastrophic results such as rubbing or even scrapping in generators. Consequently, numerous approaches have been proposed to

* Corresponding author.

E-mail address: tengw@ncepu.edu.cn (W. Teng).

detect bearing fault in generator. Mathew and Alfredson [7] reviewed the bearing fault signatures with a view to detecting incipient failure based on vibration measurements. Afterwards, the vibration analysis for bearings was extended and supplemented continually [8–10]. Kusiak and Verma [11] used historical temperature measurements to develop a neural network and predicted over-temperature faults of bearings up to 1.5 h before their occurrence. Onel and Benbouzid [12] applied Park transform and Concordia transform of stator current to find the bearing fault feature in induction motors. Bulter [13] described a shock pulse method (similar to vibration analysis) to detect faults in rolling bearings. Shiroishi et al. [14] investigated the severity and location of a bearing defect using acoustic emission. Tandon [15] analyzed several techniques above and summarized the limit size of defect that can be detected by different methods.

Comparing the aforementioned methods of defect detection, vibration analysis is the most direct and effective way for bearing condition monitoring in wind turbine generators since it can make a compromise between equipment cost and diagnosis accuracy. Massive processing methods for vibration signal were applied to detect bearing fault. Commonly, demodulation analysis combined with band-pass filtering were regarded as a classic tool to detect the modulation components hidden in the resonance frequency band [16,17]. However, the selection of the resonance band needs human interference, which results in inaccurate diagnosis. To this end, Antoni and Randall [18] proposed spectral kurtosis which can decompose signal into different frequency bands and regard the band with maximum kurtosis as the optimal filtering band. To evidence the fault impact of bearings in vibration signals, an autoregressive model and minimum entropy deconvolution were developed to restrain the periodic components from gear mesh and background noise [19,20]. Borghesani et al. applied the cepstrum pre-whitening proposed by Randall [21] to diagnose bearing faults under variable speed conditions [22]. Rai and Mohanty [23] detected bearing fault using FFT and Hilbert-Huang transform based on the ability of nonstationary signal processing. Park et al. [24] proposed the minimum variance based cepstrum for early fault detection in automotive ball bearings.

In real industry application, the statistics of the vibration signal correlating to a faulty bearing are generally periodic, and the signal is identified as cyclostationary due to random slips, speed fluctuations, and variations of the axial to radial load ratio. Antoni [25] discussed three propositions of cyclostationary analysis in rotating machines and promoted them more applicable in practice [26]. Bearing fault detection [27], Gear degradation indication [28], and other applications in pumps and diesel engines etc. [29] have validated the capability of cyclostationary analysis. However for wind turbines, researchers preferred to employ nonstationary methods to analyze gear or bearing faults such as wavelet analysis [30], empirical mode decomposition [31] etc., rather than cyclostationary analysis. In this paper, an intrinsic electromagnetic vibration (EV) in wind turbine generators, caused by an alternating magnetic field acting on a low stiffness stator, is investigated. This EV can modulate the vibration signal of the generator and impede the fault feature extraction of bearings. The demodulation ability of cyclostationary analysis is discussed. A cyclic coherence function based on cyclostationary analysis is applied to detect bearing fault in a wind turbine generator under intensive EV.

The organization of this paper is as follows. The principle of double fed induction generators and the characteristics of wind turbine drive trains are introduced in Section 2. The intrinsic electromagnetic vibration in wind turbine generator is deduced in Section 3. In Section 4, second order cyclostationary analysis is reviewed, and the corresponding spectral correlation density with cyclic coherence function are estimated. In Section 5, a real 2 MW wind turbine with a faulty bearing in its generator is tested, the vibration signals are analyzed using cyclic coherence function, complex wavelet transform and spectral kurtosis. The failure mechanism of the bearing is discussed. The conclusion is drawn in Section 6.

2. Double fed induction generator

The gearbox driven wind turbine is the main type within the category of horizontal axis wind turbines whose drive train is shown as in Fig. 1a. Stochastic winds are absorbed by blades and wind energy is converted into mechanical energy in the rotor hub with low rotational speed, then the low rotational speed is accelerated through the gearbox to drive the generator with high speed. The gearbox, which consists of a planetary stage (a sun gear, planet gears, and a ring gear) and two stages of ordinary gears, has both compact structure and large transmission ratio. The blades and rotor hub are supported by the main bearing. According to the characteristics of the drive train, acceleration transducers are attached on seven different positions to monitor the health states of the gears and bearings shown in Fig. 1a.

The double fed induction generator (DFIG) is employed comprehensively in gearbox driven wind turbines, whose operation mode is shown in Fig. 1b. The stator windings are connected to a power grid directly through a transformer, and active power is transferred all through from the stator to grid. Unlike stator windings, rotor windings are connected to the power grid using an inverter that can regulate slip power on the basis of the rotational speed of the rotor. If this rotational speed is lower than the synchronous speed of the generator, rotor absorbs power from the grid. On the contrary, rotor sends power to the grid at ultra-synchronous speed.

3. Electromagnetic vibration in wind turbine generators

Electromagnetic vibration (EV) is an intrinsic phenomenon originated from alternating deformation of the stator of generators. As shown in Fig. 2a, the three phase currents in stator windings are denoted by i_A , i_B and i_C , among which there are 120° phase differences. The three phase windings are placed symmetrically shown as in Fig. 2b to e where AX denotes A phase, BY denotes B phase and CZ denotes C phase. A, B and C in Fig. 2b–e are defined as input directions when the corresponding currents are positive. Otherwise, A, B and C are output directions when the currents are negative.

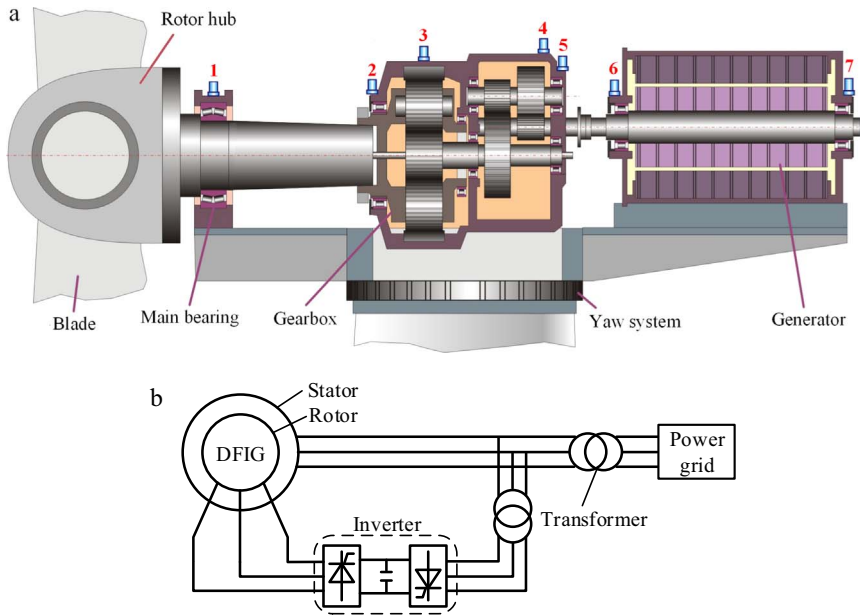


Fig. 1. Principle of double fed induction generator: (a) wind turbine drive train, (b) operation mode of DFIG.

At time *b* in Fig. 2a, $i_A=0$, $i_B < 0$, $i_C > 0$, and the directions of three phase current in stator windings are shown as in Fig. 2b. Based on electromagnetism theory, there is a magnetic field from N to S pole which leads to the attraction of different two poles mutually. Further, deformation arises if the stiffness of hollow stator is not high enough, which can be illustrated by comparing the dashed circle with solid ellipse. With the three phase currents varying to time *c*, *d* and *e*, the magnetic field and stator deformation are shown as in Fig. 2c, d and e respectively. During the half period of the alternating current from Fig. 2b–e, the magnetic field rotates 180°, and the deformation of stator varies for a whole period. That is to say, the frequency of stator deformation is twice the one of the alternating current.

Although wind speed and the rotational speed of rotor hub fluctuate, the frequency in power grid is constant due to the regulation of inverter. As depicted in Fig. 1b, the frequency of the alternating current in stator windings is equal to the one of the power grid, which is 50 Hz in China. So the frequency of the EV is 100 Hz. The same conclusion can be drawn for generator with multiple pole pairs. A typical EV from a real wind turbine generator is shown as in Fig. 3a where the evident shock intervals of 0.01 s are modulating high frequency vibration signal. Fig. 3b is the corresponding envelope spectrum which exhibits the EV of 100 Hz and 200 Hz distinctly.

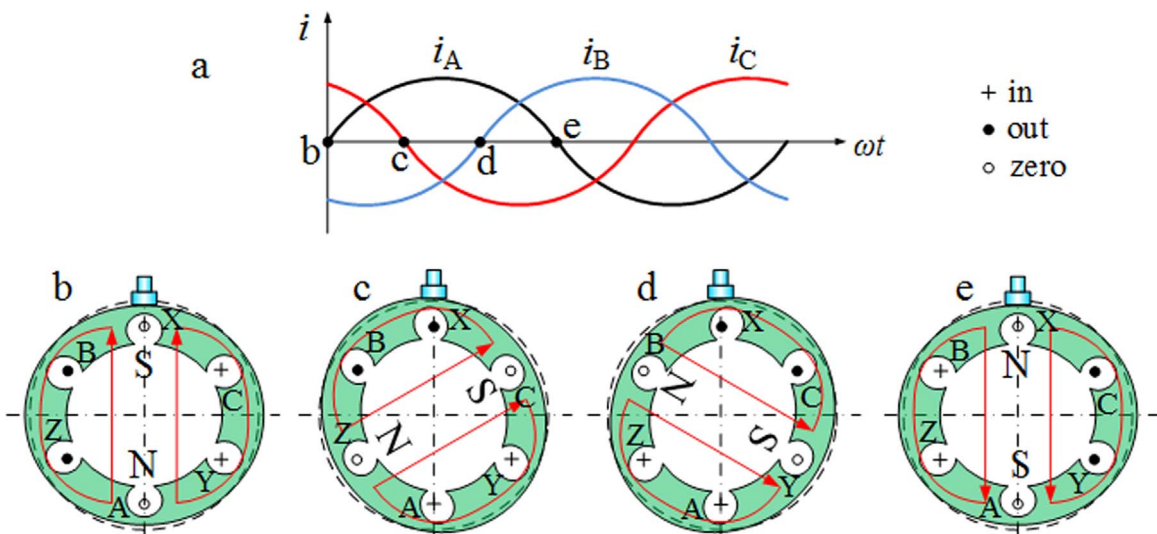


Fig. 2. Electromagnetic vibration of a generator stator: (a) three phase alternating currents, (b) magnetic field and deformation at time *b*, (c) magnetic field and deformation at time *c*, (d) magnetic field and deformation at time *d*, (e) magnetic field and deformation at time *e*.

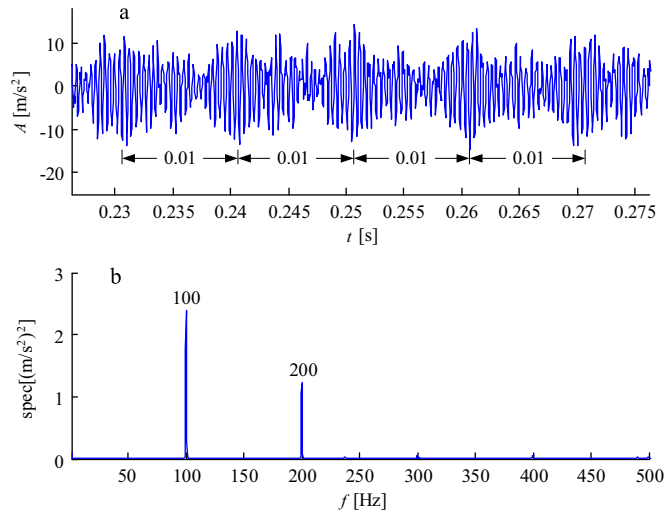


Fig. 3. Electromagnetic vibration of a generator: (a) temporal signal, (b) envelope spectrum.

4. Cyclostationary analysis and its demodulation ability

4.1. Definition

Second order cyclostationary (CS2) analysis is an effective tool to demodulate fault information buried in rotating machineries due to the cyclostationarity of fault signals. Gardner [32–34] proposed spectral redundancy and spectral correlation that can be applied in analyzing astronomical, biomedical, econometric signals etc. Afterwards, Antoni [25,26] promoted the CS2 more applicable for mechanical systems in practice, such as fault diagnosis of rolling-element bearings [27], gears degradation indication [28]. An instantaneous auto-correlation function with a symmetric structure is defined as

$$R_x(t, \tau) = E \left\{ x \left(t + \frac{\tau}{2} \right) x^* \left(t - \frac{\tau}{2} \right) \right\} \tag{1}$$

where τ is time lag. The auto-correlation function above should be periodic with cyclic period T

$$R_x(t, \tau) = R_x(t + T, \tau) \tag{2}$$

According to Fourier series, $R_x(t, \tau)$ is composed as

$$R_x(t, \tau) = \sum_{m=-\infty}^{\infty} R_x^\alpha(\tau) e^{j2\pi m t / T} = \sum_{m=-\infty}^{\infty} R_x^\alpha(\tau) e^{j2\pi \alpha t} \tag{3}$$

where $\alpha = m/T$ is cyclic frequency, $R_x^\alpha(\tau)$ is cyclic auto-correlation function and it is also the Fourier coefficient of periodic function $R_x(t, \tau)$. $R_x^\alpha(\tau)$ can be calculated as

$$R_x^\alpha(\tau) = \frac{1}{T} \int_{-T/2}^{T/2} R_x(t, \tau) e^{-j2\pi \alpha t} dt \tag{4}$$

Actually, the cyclic period T is not known accurately. Therefore, with T tending to infinite, the cyclic auto-correlation function will be continuous in cyclic frequency domain

$$R_x^\alpha(\tau) = \lim_{T \rightarrow \infty} \frac{1}{T} \int_{-T/2}^{T/2} x \left(t + \frac{\tau}{2} \right) x^* \left(t - \frac{\tau}{2} \right) e^{-j2\pi \alpha t} dt = \langle x \left(t + \frac{\tau}{2} \right) x^* \left(t - \frac{\tau}{2} \right) e^{-j2\pi \alpha t} \rangle_t \tag{5}$$

where the $\langle \rangle_t$ denotes inner product operation and the upper mark * is conjugated operator. Then cyclic auto-correlation function is converted to spectral correlation density using Fourier transform in frequency domain, which is shown as

$$S_x^\alpha(f) = \int_{-\infty}^{\infty} R_x^\alpha(\tau) e^{-j2\pi f \tau} d\tau \tag{6}$$

4.2. Estimation of spectral correlation density and cyclic coherence function

$R_x^\alpha(\tau)$ is rewritten as [35]

$$R_x^\alpha(\tau) = \left\langle \left[\left[x\left(t + \frac{\tau}{2}\right) e^{-j\pi\alpha\left(t + \frac{\tau}{2}\right)} \right] \left[x\left(t - \frac{\tau}{2}\right) e^{j\pi\alpha\left(t - \frac{\tau}{2}\right)} \right]^* \right] \right\rangle_t \tag{7}$$

Here, two variables are defined as

$$\begin{cases} u(t) = x(t)e^{-j\pi\alpha t} \\ v(t) = x(t)e^{j\pi\alpha t} \end{cases} \tag{8}$$

Substituting Eq. (8) into Eq. (7), and the expression in Eq. (7) is changed as

$$\begin{aligned} R_x^\alpha(\tau) &= \langle u\left(t + \frac{\tau}{2}\right)v^*\left(t - \frac{\tau}{2}\right) \rangle_t \\ &= \lim_{T \rightarrow \infty} \frac{1}{T} \int_{-T/2}^{T/2} u\left(t + \frac{\tau}{2}\right)v^*\left(t - \frac{\tau}{2}\right) dt \end{aligned} \tag{9}$$

$R_x^\alpha(\tau)$ in Eq. (9) is the cross-correlation of $u(t)$ and $v(t)$. By comparison, the convolution between $u(\tau)$ and $v(\tau)$ with symmetric structure is described as

$$u(\tau)*v(\tau) = \lim_{T \rightarrow \infty} \frac{1}{T} \int_{-T/2}^{T/2} u\left(t + \frac{\tau}{2}\right)v^*\left(\frac{\tau}{2} - t\right) dt \tag{10}$$

And the convolution between $u(\tau)$ and $v(-\tau)$ is calculated as

$$\begin{aligned} u(\tau)*v(-\tau) &= \lim_{T \rightarrow \infty} \frac{1}{T} \int_{-T/2}^{T/2} u\left(t + \frac{\tau}{2}\right)v^*\left(-\left(\frac{\tau}{2} - t\right)\right) dt \\ &= \lim_{T \rightarrow \infty} \frac{1}{T} \int_{-T/2}^{T/2} u\left(t + \frac{\tau}{2}\right)v^*\left(t - \frac{\tau}{2}\right) dt \end{aligned} \tag{11}$$

Comparing Eq. (9) with Eq. (11), $R_x^\alpha(\tau)$ is equal to the convolution of $u(\tau)$ and $v(-\tau)$. Based on the equivalence relation between convolution in time domain and product in frequency domain, the spectral correlation density $S_x^\alpha(f)$ which is the Fourier transform of $R_x^\alpha(\tau)$ can be calculated as

$$S_x^\alpha(f) = \lim_{T \rightarrow \infty} \frac{E\{U_T(f) \cdot V_T^*(f)\}}{T} \tag{12}$$

where E is the expectation operator, and

$$\begin{cases} U_T(f) = F\{u(t)\} = X_T\left(f + \frac{\alpha}{2}\right) \\ V_T(f) = F\{v(t)\} = X_T\left(f - \frac{\alpha}{2}\right) \end{cases} \tag{13}$$

F denotes the Fourier transform operator, and $X_T(f)$ is the Fourier transform of $x(t)$ over the time interval T .

$$X_T(f) = \int_T x(t)e^{-j2\pi ft} dt \tag{14}$$

Then the cyclic coherence function (CCF) [26] is defined as

$$C_x^\alpha(f) = \frac{E\{U_T(f) \cdot V_T^*(f)\}}{\sqrt{E\{|U_T(f)|^2\} \cdot E\{|V_T(f)|^2\}}} \tag{15}$$

$C_x^\alpha(f)$ in Eq. (15) represents the correlation of the power spectrum $X_T(f)$ at $f+\alpha/2$ and $f-\alpha/2$. Due to the cyclostationarity of fault information from bearings, $C_x^\alpha(f)$ can enhance the amplitudes at cyclic frequency α denoting fault frequency and restrain the ones at α denoting noise. Therefore, CCF is more suitable for the fault extraction of bearings than cyclic spectral density.

For fault diagnosis of generators, a cyclostationarity ratio indicating the strength of a fault feature over the EV is defined as

$$C_r(f) = \frac{\max(C_x^{\alpha_F \pm \Delta\alpha_F}(f))}{\max(C_x^{\alpha_E \pm \Delta\alpha_E}(f))} \tag{16}$$

where α_F is the theoretical cyclic frequency of fault feature, and α_E is the theoretical cyclic frequency of electromagnetic vibration. Two tiny variables $\Delta\alpha_F$ and $\Delta\alpha_E$ are introduced to compensate the inconformity between the theoretical cyclic frequency and actual one. The optimal slice frequency f_o which can display the fault feature clearly is computed as

$$f_o = \underset{f}{\operatorname{argmax}}(C_r(f)) \tag{17}$$

4.3. Simulated modulation signal

When defect arises in bearings or gears, there exists modulation phenomenon that certain natural frequency of mechanical system is carrier wave modulated by the fault feature. Demodulation analysis is effective to separate fault feature from carrier

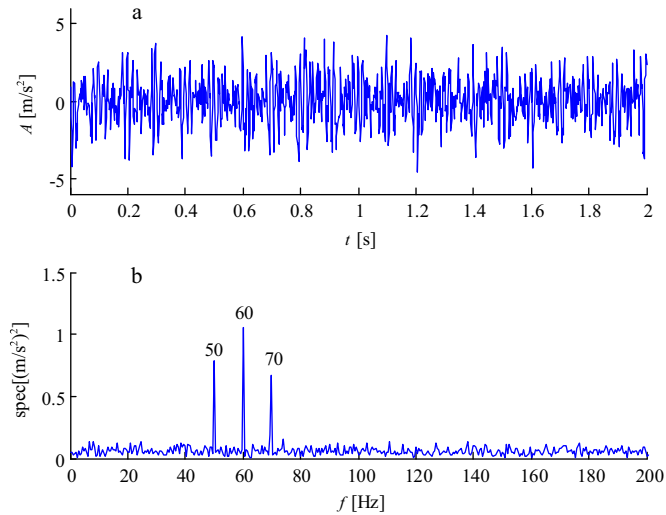


Fig. 4. Simulated modulation signals: (a) temporal signal, (b) power spectrum.

component. Antoni [29] demonstrated CS2 had a similar demodulation ability to the multiple channels band-pass filtering combined with squared envelope. Therefore, CS2 is suitable for demodulating vibration signal and detecting fault feature. Take the amplitude modulated signal $x(t) = (1 + 1.5 \cos(2\pi \cdot 10t))\cos(2\pi \cdot 60t + \pi/6) + n(t)$ to be analyzed using CS2, where the carrier frequency is 60 Hz, the modulation frequency is 10 Hz and $n(t)$ denotes a random noise [36]. The simulated modulation signal and its power spectrum are shown as in Fig. 4 where carrier frequency 60 Hz, sidebands 50 Hz and 70 Hz are distinct.

Fig. 5 is the cyclic coherence function of the amplitude modulation signal. At low frequency region, the modulation frequency 10 Hz and its harmonics can be found. Synchronously, the carrier frequency 120 Hz (two times of 60 Hz) and sidebands (100 Hz, 110 Hz, 130 Hz and 140 Hz) representing modulation components are evident at relative high frequency region. The slices of CCF at $f=60$ Hz and at $f=10$ Hz in Fig. 6 further highlight the modulation components, and verify the demodulation ability of CS2 for amplitude modulated signal.

In actual application, in order to improve the calculate efficiency of the CCF, the interval Δf in frequency domain should be large enough while the $\Delta \alpha$ in cyclic frequency domain should be small enough to guarantee the calculation precision.

In Fig. 4b, the power spectrum can detect the sideband frequencies denoting the modulation components. However, the sidebands are usually not clear in a real industrial environment under intensive background noise. CCF in Fig. 6b can also detect the sideband frequencies, more importantly than this, CCF is capable of extracting the modulation components directly in the low frequency band, which is shown in Fig. 6a.

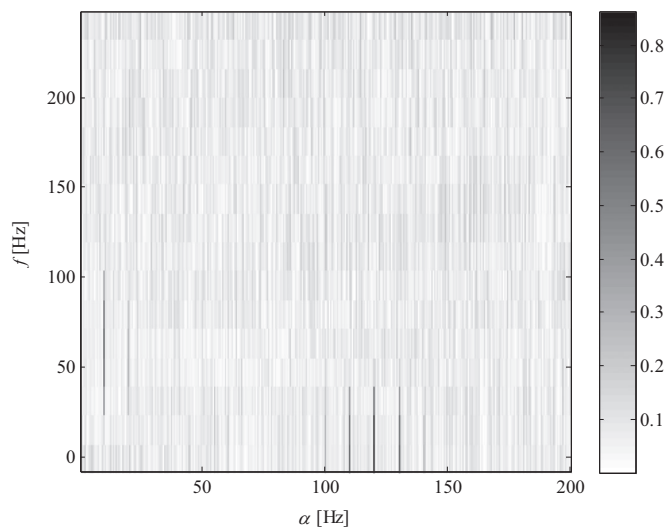


Fig. 5. Cyclic coherence function of simulated modulation signal.

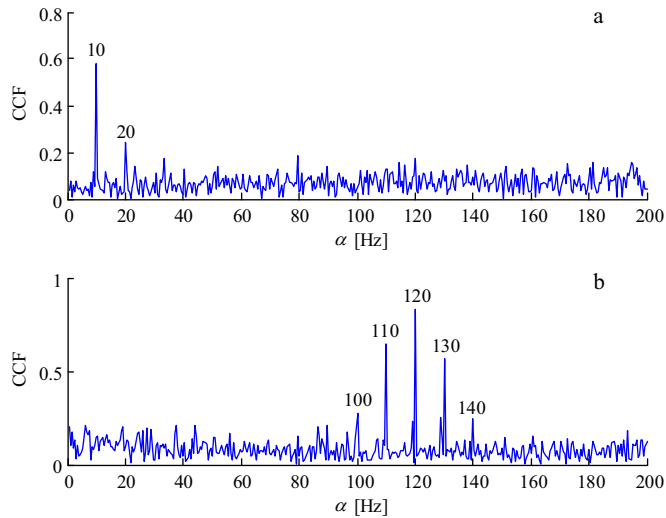


Fig. 6. Slices of CCF at different frequencies: (a) at $f=60$ Hz, (b) at $f=10$ Hz.

5. Testing and analysis for wind turbine generator

5.1. Testing condition

The rated power of the tested wind turbine is 2 MW. Its whole drive train is shown as in Fig. 1a. The acquisition system of SKF with a piezoelectric acceleration transducer were used to collect vibration signals from the drive end and non-drive end of the generator one by one, which are shown as in Fig. 7. The sensitivity of the acceleration transducers is 100 mV/g and the sampling frequency is 25,600 Hz. While testing the wind speed is 14 m/s and the rotational speed of generator is 1662 r/min ($f_r=27.7$ Hz). The tested generator is double fed induction generator with two pole pairs. The fault feature frequencies of two bearings in wind turbine generator are listed in Table 1 where f_r denotes the rotational frequency of the generator, FTF is the fundamental train frequency, BSF is the ball spin frequency of rolling element, BPFO is the ball pass frequency of outer race, and BPFI is the ball pass frequency of inner race.

5.2. Testing analysis

Fig. 8a shows the temporal vibration signal in generator drive end and its limit approaches ± 500 m/s² exceeding more than the VDI 3834 standard [37]. Fig. 8b is the temporal signal in non-drive end whose vibration range is less than Fig. 8a. Although VDI 3834 cannot be regarded as a diagnosis criteria, the excessive vibration amplitudes in Fig. 8a indicate an abnormal health condition in the drive end of generator. For comparison, the temporal signals seven months ago when this wind turbine operated well are shown as in Fig. 8c and d where the lower vibration levels are exhibited.

Except for excessive vibration amplitudes in Fig. 8a, it is difficult to find any fault information about the generator. Thus, the vibration signal in drive end is converted into frequency domain, which are shown as in Fig. 9b and c, corresponding to the linear spectrum and logarithm spectrum respectively. The vibration energy concentrates on two frequency bands shown in Fig. 9b and c.

Generally, fault information such as a bearing crack or gear broken is hidden in predominant frequency bands e.g. band 1 and band 2 in Fig. 9. Conventional band-pass filtering combined with hilbert transform are significant methods of demodulation analysis

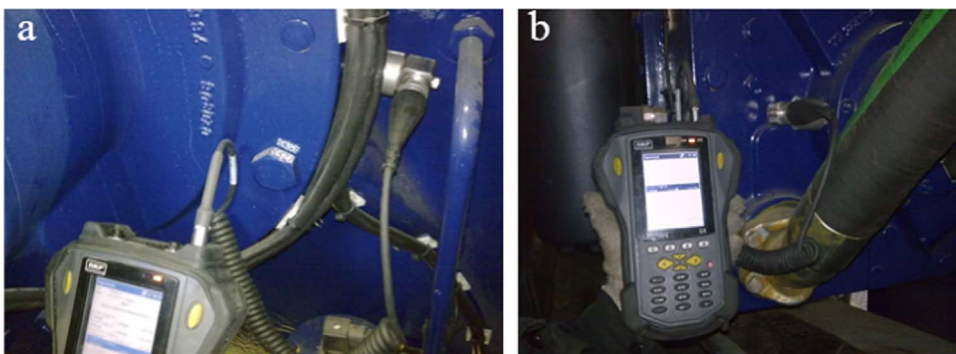


Fig. 7. Test system on field wind turbine generator: (a) drive end, (b) non-drive end.

Table 1
Bearing feature frequencies in generator.

	f_r	FTF	BSF	BPFO	BPFI
Ratio with f_r	1	0.399	2.37	3.59	5.41
Feature frequencies (Hz)	27.7	11.05	65.6	99.4	149.8

to detect fault feature. Here, two four-order Butterworth band-pass filters are used to filter the vibration signal. The envelope signals with their spectra from band 1 and band 2 in Fig. 9 are separately shown as in Fig. 10 and Fig. 11. There are evident 100 Hz and its harmonics in Fig. 10b and Fig. 11b denoting the electromagnetic vibration in the stator of generator. And the rotational frequency 27.73 Hz with its two-order harmonic 55.47 Hz are also shown in Fig. 11b. The phenomenon above illustrates that conventional demodulation analysis does not find fault components effectively because intensive EV may masks the fault feature of the bearing in this generator.

Then the vibration signal in Fig. 8a is processed using second order cyclostationary analysis, and the cyclic coherence function is shown as in Fig. 12. Besides the distinct 100 Hz with its harmonics and rotational frequency 27 Hz, the frequency component about 150 Hz is also manifest, which accords with the feature frequency of inner race in Table 1. According to Eqs.(16) and (17), the optimal frequency used to slice the CCF is 9500 Hz. The slices of the cyclic coherence function at $f=600$ Hz and $f=9500$ Hz are shown as in Fig. 13a and b where the rotational frequency 27.63 Hz and the ball pass frequency of inner race 149 Hz are evidenced. There is also a sideband component 121.4 Hz that is a 27.6 Hz interval from 149 Hz in Fig. 13b. As is known universally, when defect arises on the inner race of a bearing, the balls strike the defective part on inner race which can introduce a shock with an interval of the reciprocal of the BPFI. Meanwhile, the vibration shock is modulated by the rotational frequency of the shaft, with the defective part on the inner race entering into and leaving from load zone. The modulation process above tallies with the signatures detected in Fig. 12 and Fig. 13, which indicates the inner race of the bearing in drive end of the generator is faulty.

The cyclic spectral density of the vibration signal is shown in Fig. 14 where the BPFI 149 Hz and the rotational frequency 27.6 Hz are observed. However, they are hidden by the EV of 100 Hz and its harmonics, and less evident than the fault feature in Fig. 12.

Seven months ago when this wind turbine operated well, the generator was tested. The vibration signal in drive end and its cyclic coherence function are shown as in Fig. 8c and Fig. 15. Through observing the slices of CCF at $f=2000$ Hz and $f=9500$ Hz in Fig. 16, 100 Hz and its harmonics are still obvious in the healthy wind turbine, which denotes the generator has been undergoing intensive electromagnetic excitation. Through comparing Fig. 15 with Fig. 12, the analysis in Fig. 12 demonstrates that cyclic coherence function can detect the bearing defect hidden in EV due to second order cyclostationarity of the vibration signal of the faulty bearing.

The bearing in drive end of wind turbine generator was dismantled and the disassembled inner race is shown as in Fig. 17, which validate the diagnosis result correctly. After replacing a new bearing for the generator in drive end, the wind turbine was tested again. The tested vibration signal and its CCF are shown as in Fig. 18, and the slices of CCF are displayed in Fig. 19. There are still rotational frequency and EV components in Fig. 19a and b, nevertheless the fault feature frequency of the bearing disappears.

5.3. Comparison with other advanced demodulation methods

In order to compare the demodulation ability in homogeneous problem, other advanced demodulation tools involving complex wavelet transform and spectral kurtosis are used to analyze the original vibration signals.

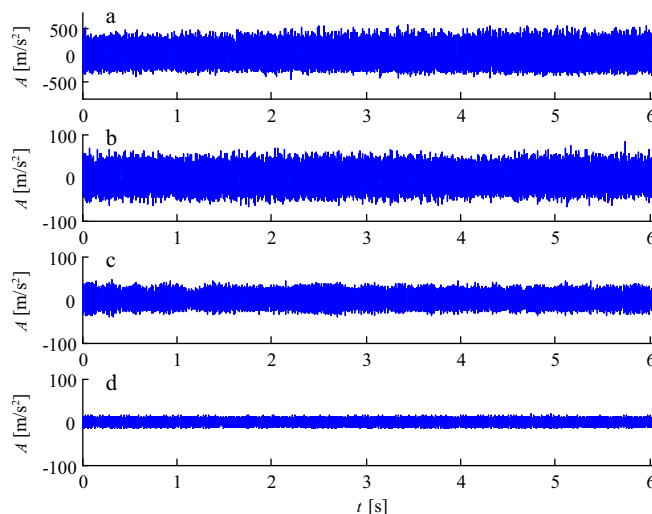


Fig. 8. Temporal vibration signals: (a) at drive end, (b) at non-drive end, (c) at drive end seven months ago, (d) at non-drive end seven months ago.

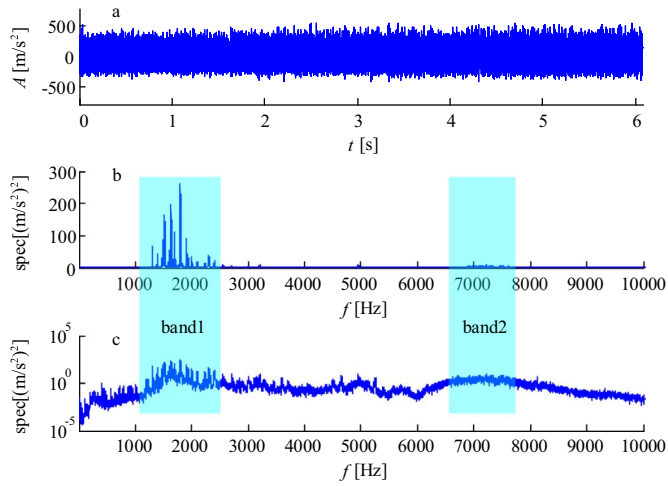


Fig. 9. Vibration signal and its power spectrum: (a) temporal signal in drive end, (b) linear power spectrum, (c) logarithm power spectrum.

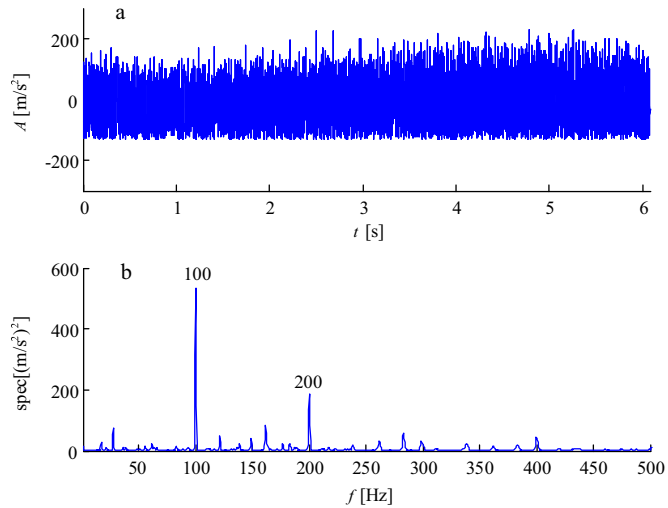


Fig. 10. Demodulation analysis for band 1: (a) envelope signal, (b) envelope spectrum.

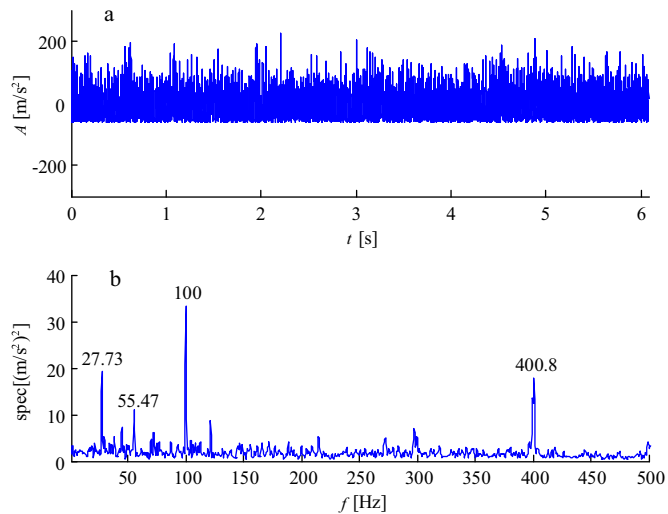


Fig. 11. Demodulation analysis for band 2: (a) envelope signal, (b) envelope spectrum.

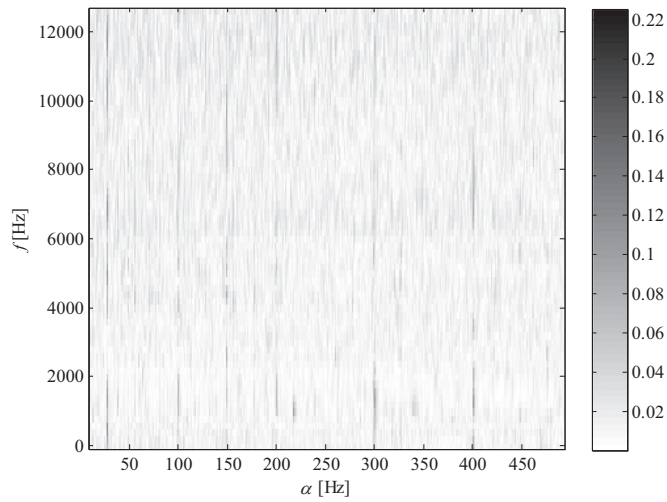


Fig. 12. Cyclic coherence function of the vibration signal.

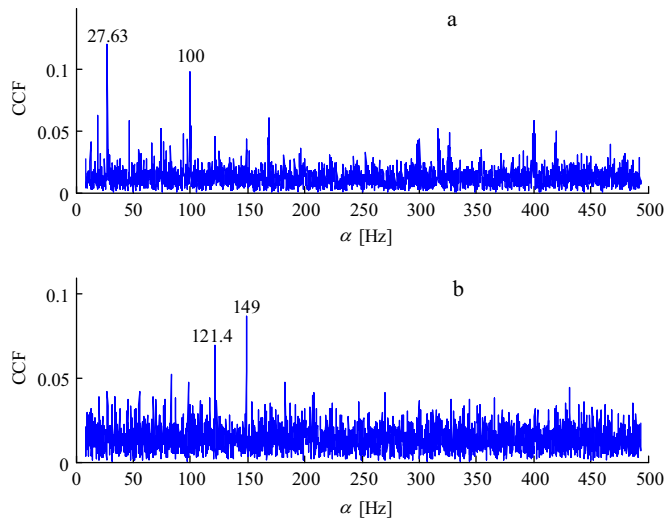


Fig. 13. Slices of the CCF: (a) slice at $f=600$ Hz, (b) slice at $f=9500$ Hz.

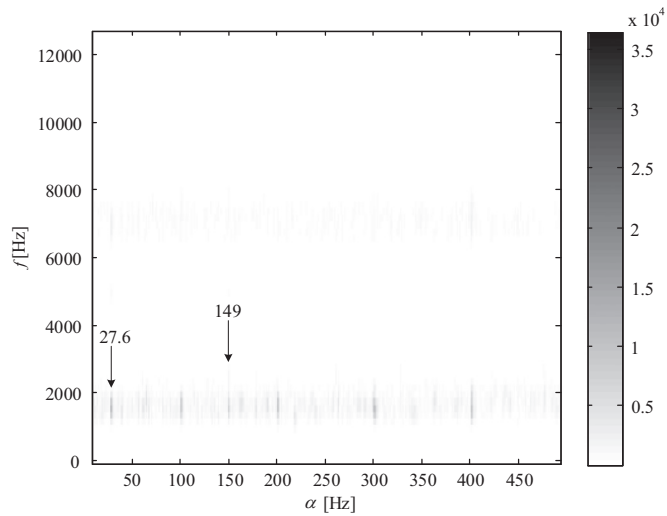


Fig. 14. Cyclic spectral density of the vibration signal.

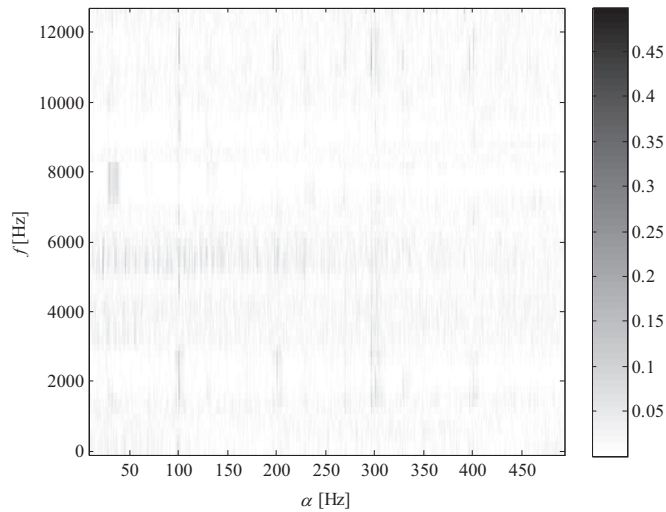


Fig. 15. Cyclic coherence function of the vibration signal seven months ago.

5.3.1. Complex wavelet transform

Complex wavelet transform enables simultaneously filtering signals at different bandwidth and obtaining a multi-scale envelope spectrum [38–40]. The multi-scale envelope spectrum and corresponding slices at different scale frequencies are shown as in Fig. 20 and Fig. 21 where the rotational frequency 27.63 Hz, electromagnetic component 100 Hz and its harmonics are clear while the BPF of bearing is hidden and neglectful. This depends on the fact that EV itself as a modulation component may disturb the extraction of bearing fault feature as depicted in Section 3. Comparing Fig. 12 with Fig. 20, the cyclic coherence function performs better than the complex wavelet transform in detecting bearing fault under intensive EV.

5.3.2. Spectral kurtosis

Spectral kurtosis is a robust method of detecting incipient faults, and can provide a unique way of designing optimal filters for filtering out the mechanical signature of faults [41] through computing the kurtosis of different frequency bands. Kurtogram, a fast computation of spectral kurtosis is developed by Antonia [42]. The vibration signal in Fig. 8a is processed by spectral kurtosis analysis, and the fast kurtogram is shown in Fig. 22. The maximal kurtosis concentrates on the center frequency 11,733.3 Hz and level 2.6, and the corresponding frequency band is 10,667–12,800 Hz. The center frequency and level of the second maximal kurtosis are 11,200 Hz and 2, having the frequency band from 9600 Hz to 12,800 Hz.

The vibration signals of the above two frequency bands are obtained by band-pass filters. Their envelope spectra are shown in Fig. 23 where the EV of 100 Hz and its harmonic are evident, as well as the rotational frequency of 27.6 Hz and its harmonic. In Fig. 23b, the BPF of 149 Hz appears, which indicates the bearing fault. However, the fault feature frequency is masked by the EV and less evident than the results of CCF in Fig. 12 and Fig. 13b.

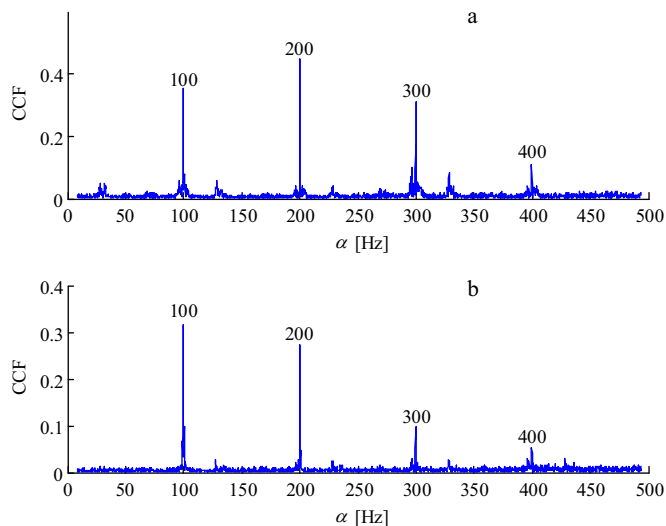


Fig. 16. Slices of CCF seven months ago: (a) slice at $f=2000$ Hz, (b) slice at $f=9500$ Hz.



Fig. 17. Bearing fault on inner race in drive end of generator.

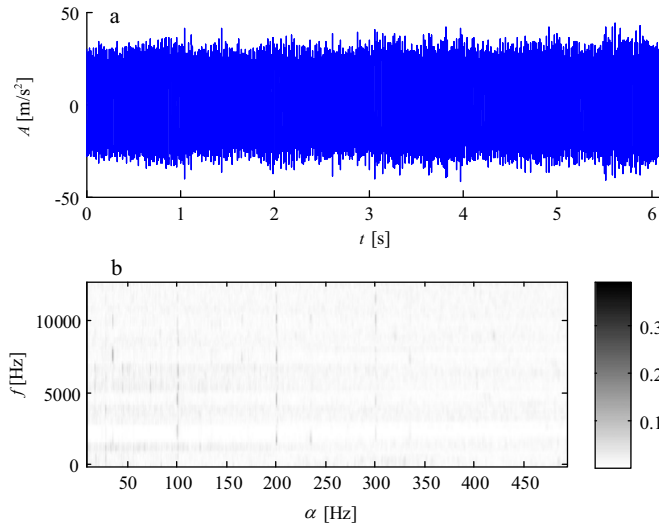


Fig. 18. Vibration signal and its cyclic coherence function after replacing the bearing: (a) vibration signal, (b) cyclic coherence function.

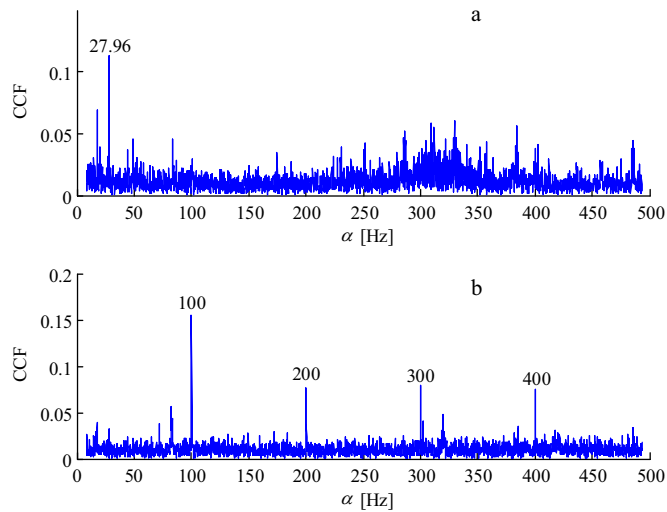


Fig. 19. Slices of CCF after replacing bearing: (a) slice at $f=600$ Hz, (b) slice at $f=9500$ Hz.

5.4. Failure mechanism and precaution suggestions

Observing the defective inner race in Fig. 17, the flutings prove that the failure may be caused by shaft current corrosion [43,44]. The mechanism of this failure type is interpreted as in Fig. 24. Due to a rotor eccentricity or unbalance of stator flux leakage in the generator, the rotor shaft may cut asymmetric magnetic field, thus generates improper induced electromotive force in shaft. The

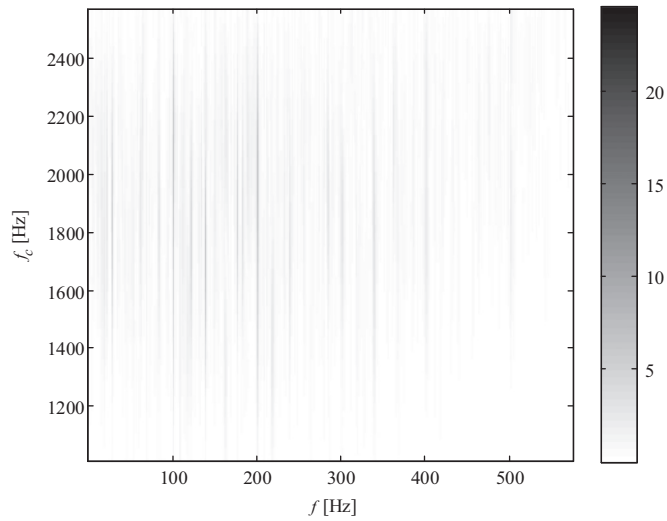


Fig. 20. Multi-scale envelope spectrum using complex wavelet transform.

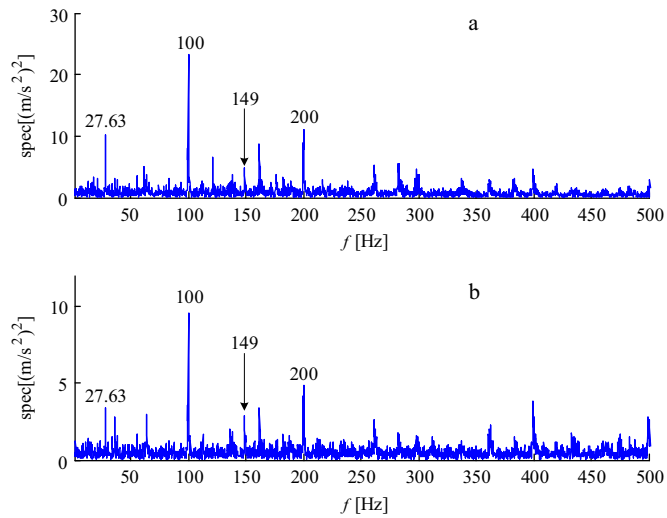


Fig. 21. Slices of multi-scale envelope spectrum: (a) at $f_c=1765.5$ Hz, (b) at $f_c=2226.1$ Hz.

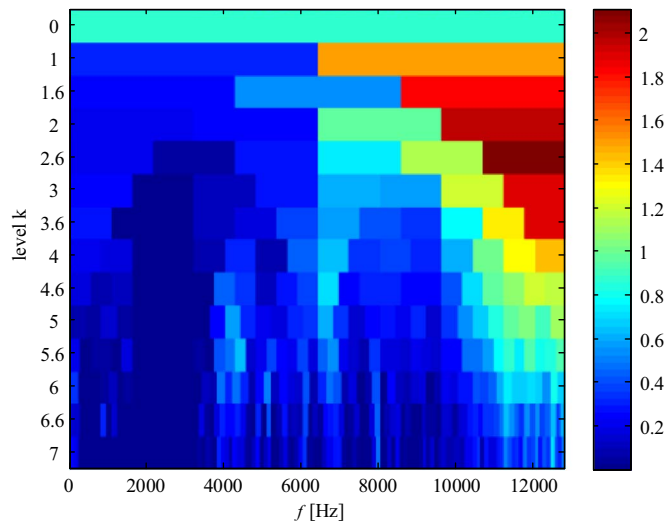


Fig. 22. Fast kurtogram of the vibration signal.

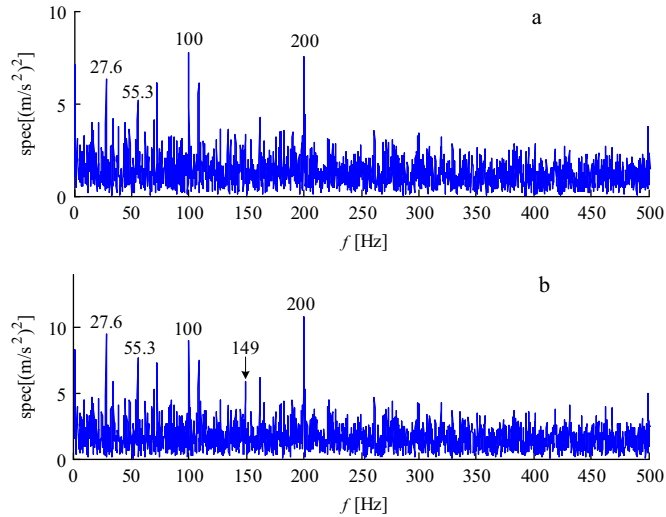


Fig. 23. Envelope spectra: (a) from the frequency band with the maximal kurtosis, (b) from the frequency band with the second maximal kurtosis.

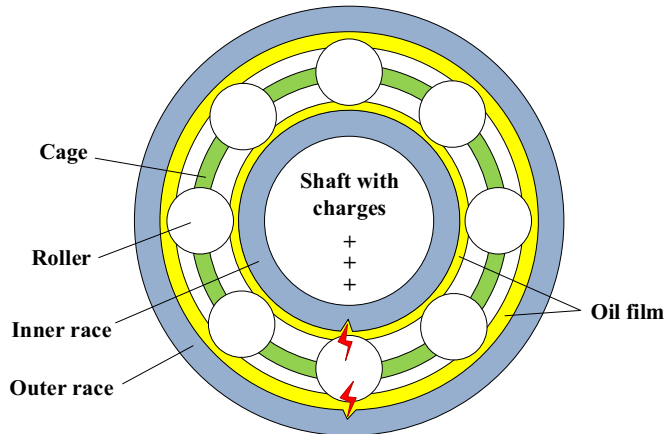


Fig. 24. Principle of shaft current corrosion.

electromotive force need a transmission path to release positive charges. If there is not ground connection, the path from shaft, inner race, ball roller, outer race to framework is a necessary choice. Theoretically, the sufficient oil film between rollers and inner or outer race can prevent the transmission of positive charges. However, once the oil film is not thick enough, rollers will contact with inner or outer race directly. Thus, due to the tiny contact point electrical discharge is inevitable and corrode inner or outer race further with the relative rolling between the roller and inner or outer race.

Shaft current corrosion is destructive for bearings in wind turbine generators. To avoid this, unhindered ground connection should be kept to guarantee shaft current releasing timely through ground wires rather than bearings. Meanwhile, excellent lubrication performance of the oil in bearing is also a pivotal factor to prevent the shaft current corrosion.

6. Conclusion

A bearing fault of real wind turbine generator has been detected successfully. In wind turbine generators, bearing faults are likely masked by intensive electromagnetic vibration of stator, which become a challenging task to extract bearing fault feature. Fortunately, cyclostationarity of the vibration signal correlating to a faulty bearing makes it available through utilizing second order cyclostationary analysis.

The EV which is a disturbance source in fault feature extraction is analyzed. Conventional band-pass filtering combined with Hilbert transform are applied to process the vibration signal from faulty bearing, but it is abortive to find bearing fault features except intensive electromagnetic components. Using cyclic coherence function based on second order cyclostationary analysis, a fault feature of inner race is evidenced among electromagnetic components. Complex wavelet transform and spectral kurtosis are adopted to compare the demodulation ability with CCF in this homogeneous problem. Unfortunately, they perform worse than CCF.

The disassembled bearing validates the effectiveness of cyclic coherence function in detecting bearing fault feature. Observing extrinsic surface of the failed inner race, the failure cause is attributed to shaft current corrosion and the failure mechanism is analyzed. Finally, the precautions are presented to prevent the shaft current corrosion from destroying bearings in wind turbine generators.

Acknowledgment

The research presented in this paper was supported by National Natural Science Foundation of China (No. 51305135), the Fundamental Research Funds for the Central Universities of China (No. 2015ZD15), Science and Technology Plan Projects of Hebei (No. 15214307D), and the National High Technology Research and Development Program of China (863 Program) (No. 2015AA043702).

References

- [1] Global Wind Report, Annual Market Update, 2015, (http://www.gwec.net/wp-content/uploads/vip/GWEC-Global-Wind-Report_2016.pdf).
- [2] M. Zeng, S. Xue, L.Y. Li, H. Cheng, G. Zhang, Wind Power Incidents in China: Investigation and Solutions, (<http://www.powermag.com/wind-power-incidents-in-china-investigation-and-solutions>), 2013.
- [3] A.A. Salem, A. Abu-Siada, S. Islam, Condition monitoring techniques of the wind turbines gearbox and rotor, *Int. J. Electr. Energy* 2 (1) (2014) 53–56.
- [4] M.R. Wilkinson, F. Spinato, P.J. Tavner, Condition monitoring of generators & other subassemblies in wind turbine drive trains, in: *Proceedings of the IEEE International Symposium on Diagnostics for Electric Machines, Power Electronics and Drives, 2007*, pp. 388–392.
- [5] F.P.G. Marquez, A.M. Tobias, J.M.P. Perez, M. Papaalias, Condition monitoring of wind turbines: techniques and methods, *Renew. Energy* 48 (2012) 110–116.
- [6] K. Alewine, W. Chen, A review of electrical winding failures in wind turbine generators, *IEEE Electr. Insul. Mag.* 28 (4) (2012) 8–13.
- [7] J. Mathew, R.J. Alfredson, The condition monitoring of rolling element bearings using vibration analysis, *J. Vib. Acoust. Stress Reliab. Des.* 106 (3) (1984) 447–453.
- [8] Y.T. Su, S.J. Lin, On initial fault detection of a tapered roller bearing: frequency domain analysis, *J. Sound Vib.* 155 (1) (1992) 75–84.
- [9] S. Orhan, N. Akturk, V. Celik, Vibration monitoring for defect diagnosis of rolling element bearings as a predictive maintenance tool: comprehensive case studies, *NDT E Int.* 39 (4) (2006) 293–298.
- [10] H. Saruhan, S. Sandemir, A. Cicek, I. Uygur, Vibration analysis of rolling element bearings defects, *J. Appl. Res. Technol.* 12 (3) (2014) 384–395.
- [11] A. Kusiak, A. Verma, Analyzing bearing faults in wind turbines: a data-mining approach, *Renew. Energy* 48 (2012) 110–116.
- [12] I.Y. Onel, M.E.H. Benbouzid, Induction motor bearing failure detection and diagnosis: Park and Concordia transform approaches comparative study, *IEEE/ASME Trans. Mechatron.* 13 (2) (2008) 257–262.
- [13] D.E. Bulter, The shock-pulse method for the detection of damaged rolling bearings, *Non-Destr. Test.* 6 (2) (1973) 92–95.
- [14] J. Shiroishi, Y. Li, S. Liang, T. Kurfess, S. Danyluk, Bearing condition diagnostics via vibration and acoustic emission measurements, *Mech. Syst. Signal Process.* 11 (5) (1997) 693–705.
- [15] N. Tandon, G.S. Yadava, K.M. Ramakrishna, A comparison of some condition monitoring techniques for the detection of defect in induction motor ball bearings, *Mech. Syst. Signal Process.* 21 (1) (2007) 244–256.
- [16] M. Feldman, Hilbert transform in vibration analysis, *Mech. Syst. Signal Process.* 25 (3) (2011) 735–802.
- [17] R.B. Randall, J. Antoni, Rolling element bearing diagnostics - a tutorial, *Mech. Syst. Signal Process.* 25 (2) (2011) 485–520.
- [18] J. Antoni, R.B. Randall, The spectral kurtosis: application to the vibratory surveillance and diagnostics of rotating machines, *Mech. Syst. Signal Process.* 20 (2) (2006) 308–331.
- [19] R. Li, P. Sopon, D. He, Fault features extraction for bearing prognostics, *J. Intell. Manuf.* 23 (2) (2012) 313–321.
- [20] N. Sawalhi, R.B. Randall, H. Endo, The enhancement of fault detection and diagnosis in rolling element bearings using minimum entropy combined with spectral kurtosis, *Mech. Syst. Signal Process.* 21 (6) (2007) 2616–2633.
- [21] R.B. Randall, N. Sawalhi, M. Coats, A comparison of methods for separation of deterministic and random signals, *Int. J. Cond. Monit.* 1 (1) (2011) 11–19.
- [22] P. Borghesani, P. Pennacchi, R.B. Randall, N. Sawalhi, R. Ricci, Application of cepstrum pre-whitening for the diagnosis of bearing faults under variable speed conditions, *Mech. Syst. Signal Process.* 36 (2) (2013) 370–384.
- [23] V.K. Rai, A.R. Mohanty, Bearing fault diagnosis using FFT of intrinsic mode functions in Hilbert-Huang transform, *Mech. Syst. Signal Process.* 21 (6) (2007) 2607–2615.
- [24] C.S. Park, Y.C. Choi, Y.H. Kim, Early fault detection in automotive ball bearings using the minimum variance cepstrum, *Mech. Syst. Signal Process.* 38 (2) (2013) 534–548.
- [25] J. Antoni, F. Bonnardot, A. Raad, M.E. Badaoui, Cyclostationary modelling of rotating machine vibration signals, *Mech. Syst. Signal Process.* 18 (6) (2004) 1285–1314.
- [26] J. Antoni, Cyclic spectral analysis in practice, *Mech. Syst. Signal Process.* 21 (2) (2007) 597–630.
- [27] J. Antoni, Cyclic spectral analysis of rolling-element bearing signals: facts and fictions, *J. Sound Vib.* 304 (3–5) (2007) 497–529.
- [28] A. Raad, J. Antoni, M. Sidahmed, Indicators of cyclostationarity: theory and application to gear fault monitoring, *Mech. Syst. Signal Process.* 22 (3) (2008) 574–587.
- [29] J. Antoni, Cyclostationarity by examples, *Mech. Syst. Signal Process.* 23 (4) (2009) 987–1036.
- [30] Z. Hameed, Y.S. Hong, Y.M. Cho, S.H. Ahn, C.K. Song, Condition monitoring and fault detection of wind turbines and related algorithms: a review, *Renew. Sustain. Energy Rev.* 13 (1) (2009) 1–39.
- [31] W. Teng, F. Wang, K.L. Zhang, Y.B. Liu, X. Ding, Pitting fault detection of a wind turbine gearbox using empirical mode decomposition, *Stroj. Vestnik J. Mech. Eng.* 60 (1) (2014) 12–20.
- [32] W.A. Gardner, Exploitation of spectral redundancy in cyclostationary signals, *IEEE Signal Process. Mag.* 8 (2) (1991) 14–36.
- [33] W.A. Gardner, Measurement of spectral correlation, *IEEE Trans. Acoust. Speech Signal Process.* 34 (5) (1986) 1111–1123.
- [34] W.A. Gardner, The spectral correlation theory of cyclostationary time-series, *Signal Process.* 11 (1) (1986) 13–36.
- [35] X.D. Zhang, Z. Bao, *Nonstationary Signal Analysis and Processing*, National Defense Industry Press, Beijing, China, 1998.
- [36] Z.J. He, Y.Y. Zi, X.N. Zhang, *Modern Signal Processing and its Application in Engineering*, Xi'an Jiaotong University Press, Xi'an, China, 2007.
- [37] VDI 3834, Measurement and Evaluation of the Mechanical Vibration of Wind Energy Turbines and Their Components Onshore Wind Energy Turbines with Gears, 2009, p. 16.
- [38] R.Q. Yan, R.X. Gao, Multi-scale enveloping spectrogram for vibration analysis in bearing defect diagnosis, *Tribol. Int.* 42 (2) (2009) 293–302.
- [39] J.J. Wang, R.X. Gao, R.Q. Yan, Multi-scale enveloping order spectrogram for rotating machine health diagnosis, *Mech. Syst. Signal Process.* 46 (1) (2014) 28–44.
- [40] W. Teng, X. Ding, X.L. Zhang, Y.B. Liu, Z.Y. Ma, Multi-fault detection and failure analysis of wind turbine gearbox using complex wavelet transform, *Renew. Energy* 93 (2016) 591–598.
- [41] J. Antonia, R.B. Randall, The spectral kurtosis: application to the vibratory surveillance and diagnostics of rotating machines, *Mech. Syst. Signal Process.* 20 (2) (2006) 208–331.
- [42] J. Antonia, Fast computation of the kurtogram for the detection of transient faults, *Mech. Syst. Signal Process.* 21 (1) (2007) 108–124.
- [43] D. Busse, J. Erdman, R.J. Kerkman, D. Schlegel and G. Skibinski, An evaluation of the electrostatic shielded induction motor: asolution for rotor shaft voltage buildup and bearing current, in: *Industry Applications Conference, Thirty-First IAS Annual Meeting, IAS '96, 1996*, pp.610-617
- [44] R.F. Schiferl, M.J. Melfi, Bearing current remediation options, *IEEE Ind. Appl. Mag.* 10 (4) (2004) 40–50.